Engineering Fracture Mechanics 268 (2022) 108475

Contents lists available at ScienceDirect

Engineering Fracture Mechanics

journal homepage: www.elsevier.com/locate/engfracmech

The role of process induced polymer morphology on the fracture toughness of titanium–PEKK interfaces

V.M. Marinosci [a,b], N.G.J. Helthuis [b], L. Chu [b,c], W.J.B. Grouve [b,*], M.B. de Rooij [b], S. Wijskamp [a], R. Akkerman [a,b]

[a] ThermoPlastic composites Research Center (TPRC), Palatijn 15, 7521PN Enschede, Netherlands
[b] University of Twente, Drienerlolaan 5, 7522NB Enschede, Netherlands
[c] State Key Laboratory of Materials-Oriented Chemical Engineering, College of Chemical Engineering, Nanjing Tech University, 211816, Nanjing, China

ARTICLE INFO

Keywords:
Toughness testing
Fractography
Polymer morphology
Interface fracture
Hybrid joints

ABSTRACT

The effect of the degree of crystallinity on the fracture toughness of titanium–PEKK interfaces was investigated experimentally. The level of crystallinity at the interface was varied by employing different processes commonly used in aerospace, namely autoclave consolidation, press-forming and annealing. The fracture toughness was assessed via the Double Cantilever Beam test, while the polymer degree of crystallinity was evaluated via Differential Scanning Calorimetry. Fracture surfaces were analyzed using confocal microscopy, SEM and AFM, to correlate the degree of crystallinity to the failure mechanisms and the toughness. The samples with a high degree of crystallinity exhibited a lower fracture toughness and a dominant cohesive failure, consisting of a combination of brittle fracture of the spherulites, and ductile fracture of the amorphous regions between the spherulites. Lowering the degree of crystallinity led to a higher fracture toughness, due to extensive plastic deformation of the amorphous polymer. In addition, fractography showed a transition from cohesive to interfacial failure in the case of a low degree of crystallinity. Our results show that the crystalline structure of the polymer has to be taken into account when optimizing the performance of metal–composite hybrid joints based on thermoplastic matrices.

1. Introduction

Joining high performance polymer composites to metals is common practice in the aerospace industry. Generally, this type of joints can be found in the form of metal inserts placed in composite structures for facilitating load introduction [1] or simply for assembly purposes [2]. Moreover, composites and metals can also be combined in the form of Fiber Metal Laminates (FMLs), which consist of thin metal layers alternated with composite plies. The resulting hybrid material is attractive in many applications as it exhibits enhanced properties such as higher fatigue, abrasion, and impact resistance compared to its constituent materials [3].

Currently, the connection between composites and metals is achieved with conventional and well-established joining techniques like mechanical fastening, adhesive bonding, or a combination of both [4]. The choice of the joining method depends on many factors, including joint geometry, type of load introduced, materials and manufacturing process employed. Typically, metal–composite joints for aerospace applications involve the combination of lightweight metals, like aluminium or titanium, with thermoset or thermoplastic-based composites.

* Corresponding author at: University of Twente, Drienerlolaan 5, 7522NB Enschede, Netherlands.
E-mail address: w.j.b.grouve@utwente.nl (W.J.B. Grouve).

https://doi.org/10.1016/j.engfracmech.2022.108475
Received 12 January 2022; Received in revised form 26 February 2022; Accepted 15 April 2022
Available online 20 April 2022

Recently, thermoplastic composites (TPCs) have gained widespread attention as they show higher toughness, longer shelf-life, and lower flammability compared to their thermoset counterparts. Additionally, the melt-processable nature of the thermoplastic matrix allows short processing time, ability to repeatedly melt and shape a part [5], and the option to recycle the material without separating fiber and matrix [6]. Furthermore, the melt-processability of TPCs enables a third joining technology, generally called co-consolidation or co-molding. This one-step method consists of joining metals and TPCs during a typical composite consolidation or forming process. The high temperatures used to process TPCs allow composite consolidation concurrently with bonding to the metal, because the thermoplastic matrix, being in a molten state, serves as the adhesive.

Since composite consolidation and insert integration occur in the same process, the additional drilling operations, associated with mechanical fastening, or the curing step required for adhesives can be avoided, thereby saving time and costs. Thus, the co-consolidation technology may represent a potential alternative to manufacture hybrid metal–composite joints more efficiently than the current standard joining technologies.

In the development of a reliable co-consolidation technology, it is essential to understand and optimize the adhesion at the metal–polymer interface. It is established that adhesion and interaction between polymers and metals can be promoted via different types of metal surface treatments prior to the bonding. Treatments like grit-blasting and laser ablation tend to modify the metal surface morphology to promote mechanical interlocking as they introduce surface cavities and irregularities [7], which are filled by the polymer during processing. Treatments like etching, anodizing, or the use of primers promote physical or chemical interaction between the two adherends [8,9].

Studies conducted on co-consolidated titanium-C/PEKK joints showed a significant improvement of the mechanical performance when grit-blasting the titanium surface [10]. Promoting the mechanical interlocking at the titanium–TPC interface causes a deflection of the failure path from the interface into the composite, with a consequent increase of the fracture toughness [11]. This result suggests that, for this type of material system, the energy to further propagate the crack also depends on properties related to the composite material, such as fiber volume fraction, fiber orientation, and polymer morphology.

When dealing with semi-crystalline polymers, it is well known that their crystalline morphology is influenced by the thermal history, e.g. the cooling rate. In turn, the morphology significantly affects the macroscopic mechanical properties of the pure polymer [12], as well as of the resulting composite material [13,14]. Typical manufacturing processes used in aerospace comprise a large variety of thermal histories. Long processes, such as autoclave or oven consolidation, are characterized by long dwell time and low cooling rates, while short processes, such as press-forming, are characterized by short dwell time and high cooling rates. As a consequence, changes in the polymer morphology induced by processing conditions may also affect the mechanical performance of metal–TPC joints. Until now, there is a limited knowledge on the interrelation between the process-induced morphology and the mechanical performance of metal–polymer interfaces. Developing a proper understanding is a fundamental step to help predict the mechanical performance of the final part and to further implement the co-consolidation technology.

The objective of this study is to experimentally investigate the relation between polymer morphology and mechanical performance of metal–polymer interfaces prepared using standard aerospace consolidation and forming processes. The material system studied consisted of a titanium alloy (Ti6Al4V) bonded to a high performance thermoplastic polymer (PEKK), both commonly used in aerospace. Our results show that the titanium–PEKK interfacial fracture toughness is strongly influenced by the polymer morphology induced by the thermal history. In addition, we provide an analysis of the mechanisms underlying the change in toughness. Understanding the interrelation between process, structure, and mechanical performance is an essential aspect to ultimately design a co-consolidation process that ensures optimal metal–TPC interfacial performance.

2. Experimental methods

2.1. Materials and metal surface preparation

Strips of grade 5 titanium (Ti6Al4V) with a thickness of 3 mm, provided by Singeling B.V., were used in this study. The surface morphology of the titanium strips was modified via grit-blasting prior to sample manufacturing, to promote the mechanical interlocking and hence, ensuring a reasonable bond [11]. First, the titanium strips were cleaned from any dust or contaminants with ethanol, in an ultrasonic bath, for 15 min at room temperature. Then, the titanium surface was grit-blasted up to an average roughness of 3 μm. The grit-blasting was carried out using alumina oxide particles (Al_2O_3) whose dimensions varied from 150 μm to 350 μm (sieve mesh number of 60). The grit-basting parameters consisted of a pressure of 4 bar, a blasting angle of 90° and a distance of 50 mm from the nozzle. After the treatment, the cleaning step in the ultrasonic bath was repeated, and then compressed air was used to further remove contaminations introduced by the grit particles.

The polymer selected was the Kepstan® 7002 PEKK (poly ether ketone ketone) produced by Arkema. It is a semi-crystalline polymer with a glass transition temperature (T_g) of about 150 °C and a melting temperature of 345 °C. It was provided as a film of 50 μm in thickness. The PEKK film was dried at 100 °C for 24 h before the sample preparation to ensure that the material did not retain any moisture.

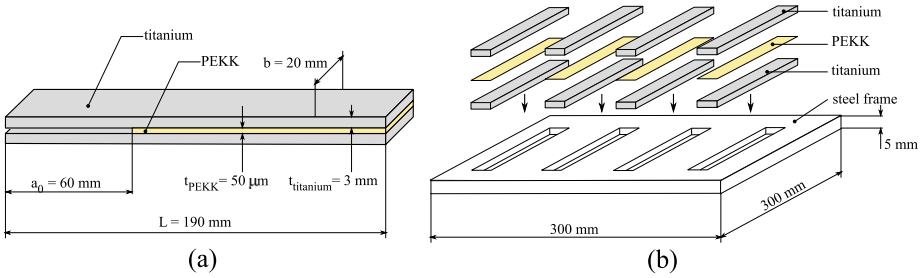

Fig. 1. (a) Geometry and dimensions of a titanium–PEKK DCB sample, (b) schematic representation of the stack and positioning in the steel frame.

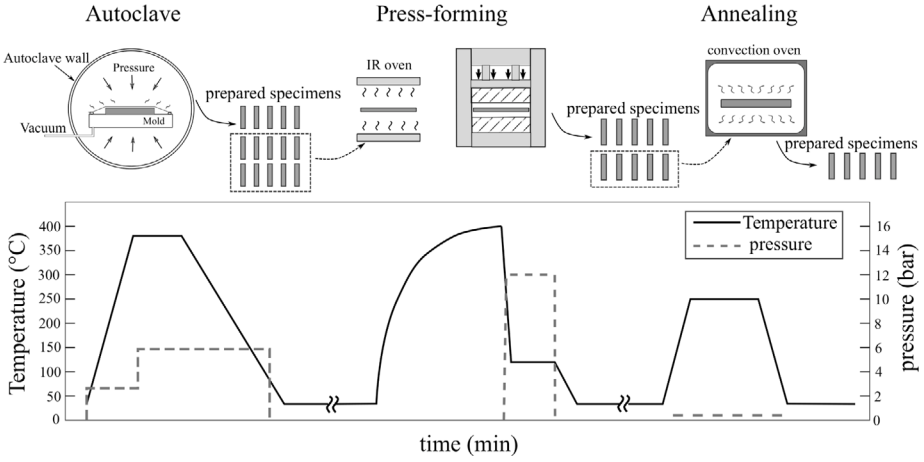

Fig. 2. Schematic overview of the different processes and relevant parameters used in the sample manufacturing (x-axis is not true to scale).

2.2. Sample preparation

The interfacial fracture toughness was assessed via Double Cantilever Beam (DCB) testing. In this work, DCB samples, whose geometry and dimensions are schematically shown in Fig. 1(a), were prepared by bonding two titanium strips using a layer of PEKK film. Each coupon, which consisted of the PEKK film sandwiched between two titanium strips, was placed in a steel frame, as represented in Fig. 1(b). The steel frame ensured a good alignment of the two titanium strips during the co-consolidation process and reduced outflow of the polymer during processing.

The DCB test requires an initial pre-crack at the interface, which was introduced by applying a mold release agent (Marbocote 227-CEE) on the first 60 mm of the titanium surface prior to consolidation. The same release agent was also applied to the steel frame to avoid bonding to the polymer.

Three types of polymer morphology, hence three sets of samples, were manufactured using three different processes. A schematic overview of the processes employed is provided in Fig. 2. The first process used was autoclave consolidation (slow process). The thermal cycle used was comparable to the cycle adopted to consolidate TPC laminates based on PEKK. First, the sample was heated up to a temperature of 375 °C and then a dwell time of 30 min and 6 bar pressure were applied. Afterwards, the system was cooled down at a constant rate of 4 °C/min. A total number of fifteen specimens was prepared, of which ten were subjected to an additional press-forming step, while the remaining five were subjected to the DCB test.

The press-forming step (fast process) consisted of re-heating the ten specimens in an infrared oven, until a temperature of 385 °C was reached. Subsequently, the system was held at a constant temperature for 5 min and then automatically transported to the forming station, where it was pressed between two flat molds at a pressure of 12 bar for 3 min. The temperature of the molds was kept at 20 °C to ensure a high cooling rate. Since the system was suspended via springs, the metal frame used in this process was made out of cast aluminium and it was placed between two 300 × 300 mm^2 aluminium caul sheets. Temperature measurements, realized with thermocouples embedded in the specimen, detected a cooling rate in the polymer layer of approximately 2000 °C/min between 385 °C and 120 °C. At the end of the press-forming step, five specimens were subjected to an annealing cycle, while the other five were subjected to the DCB test.

The annealing step was carried out in a convection oven by heating the specimens up to 250 °C and holding this constant temperature for 1 h. Afterwards, the system was cooled down at 10 °C/min. The obtained five annealed specimens were also assessed via DCB test. Notably, by first consolidating all the specimens in the autoclave, the same consolidation quality and same polymer thickness were ensured.

2.3. DCB test

The fracture toughness was evaluated via DCB test. For each sample, the mode I fracture toughness was evaluated by averaging the critical energy release rate G_{IC} of five specimens. The G_{IC} value was calculated according to the Modified Beam Theory (MBT), following the ASTM D5528 standard:

$$G_{IC} = \frac{3P\delta}{2b(a+\Delta)}, \tag{1}$$

where b is the specimen width, while P, δ and a are the force, the displacement and the delamination length respectively. The force was detected using a 2.5 kN load cell, while the displacement was evaluated via a 150 mm Linear Variable Displacement Transducer (LVDT). Loading blocks were glued at the end of each specimen, in correspondence to the pre-crack region to introduce the opening force. The tests were performed at a constant displacement rate of 3 mm/min. The delamination length was measured with a camera system that followed the position of the crack tip during the whole duration of the test. The delamination values were corrected taking into account the rotation and the deflection of the crack tip by means of the correction Δ, which was determined experimentally knowing the specimen compliance according to the ASTM D5528 standard. The compliance for different delamination lengths was determined by loading and unloading the specimen six times, following delamination increments of 10 mm each time. Subsequently, by plotting the cube root of the compliance as a function of the delamination length, a Δ value of 1.96 mm was found.

2.4. DSC experiments

The degree of crystallinity of PEKK was investigated by means of a differential scanning calorimeter from TA Instruments (DSC 250). After mechanical testing, DSC samples were obtained by scraping the polymer at random location along the crack surfaces. For each type of DCB sample, three DSC specimens were considered with a weight varying from 5 mg to 8 mg. The measurements were performed in a Nitrogen atmosphere starting with a heating step from 40 °C to 390 °C at 10 °C/min. Then, the system was cooled down to 40 °C at 4 °C/min and reheated up to 390 °C at a rate of 10 °C/min. From the first heating step, the degree of crystallinity was calculated with the following equation:

$$\chi_c = \frac{\Delta H_f - \Delta H_c}{\Delta H_{100\%}} \tag{2}$$

where ΔH_f is the melting enthalpy, ΔH_c is the enthalpy of the cold crystallization peak and $\Delta H_{100\%}$ is the melting enthalpy of fully crystallized PEKK. In this work, the fusion enthalpy of a fully crystallized PEKK was considered to be 130 J/g [15]. Besides, from the analysis of the cooling and the second heating steps, properties like glass transition and crystallization temperatures were inspected and compared to the properties of the as-received PEKK to understand whether multiple heating cycles, used during the sample manufacturing, caused any significant polymer degradation.

2.5. Microscopy analysis

Mechanical testing was followed by microscopy analysis carried out with different methods. Samples cross sections were examined to investigate the consolidation quality as well as polymer thickness. This characterization was conducted using a digital microscope (Keyence VHX-7000).

Crack surfaces were first inspected using a 3D optical profilometer (Sensofar S neox) to identify the failure mechanisms, followed by a closer inspection using a Scanning Electron Microscope (SEM Jeol JSM-7200f) to investigate the polymer microstructure at the crack surface.

SEM was complemented by Atomic Force Microscopy (AFM), conducted with a Park XE-100 AFM from Park Systems. The AFM measurements were performed in tapping mode at ambient conditions. The probe used was an ACTA AFM probe purchased from AppNano. The probe spring constant, determined with the thermal noise method, was 26 N m^{-1}. The resonance frequency used was about 300 kHz, with scan rate of 0.2 Hz. The free oscillation amplitude of the cantilever was set at 25 nm. The AFM experiments focused on recording phase-mode data, which allow to map stiffness variations on a surface, thereby to distinguish regions of different moduli [16]. In the case of a polymer surface, this method enables to identify and distinguish crystalline regions from amorphous regions, thus providing a more in depth understanding of the polymer morphology obtained [17,18].

3. Results

3.1. Interfacial fracture toughness

Fig. 3(a) shows an example of a force–displacement curve obtained during the DCB test. The plot is characterized by a linear loading behavior during the initial phase of the test, until initiation of crack extension. Then, stable crack propagation was observed in all specimens. During the unloading phase, the specimen returned to zero displacement at zero force, indicating that the thickness of the titanium arms (3 mm) was sufficient to prevent any plastic deformation. The linearity of the force vs. displacement plots, as well as the absence of significant plastic deformation justifies the use of linear elastic fracture mechanics [19].

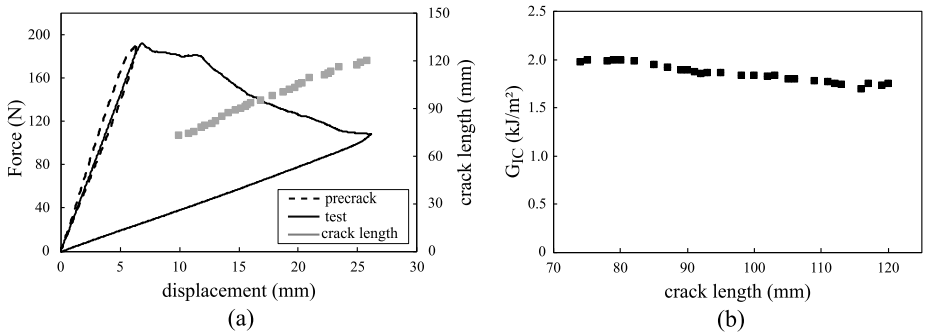

Fig. 3. (a) Typical force vs. displacement curve and crack length vs. displacement curve obtained from testing a DCB specimen, (b) Typical R-curve which shows the resistance points obtained for a single specimen.

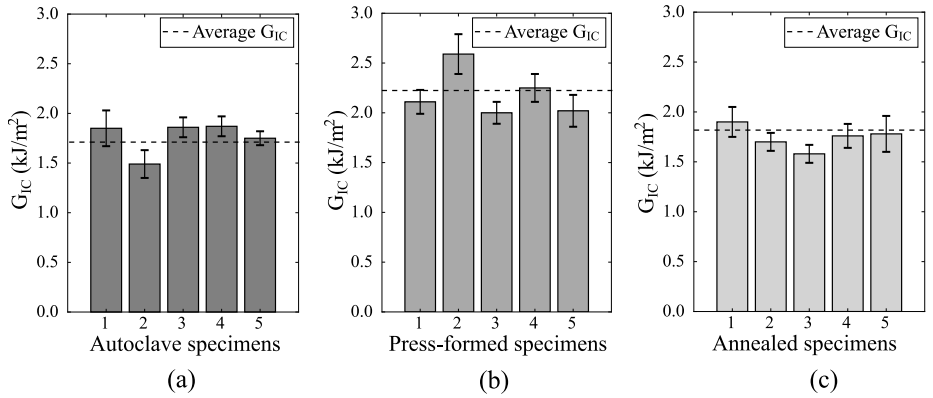

Fig. 4. Average and standard deviation of the toughness values for (a) the autoclave specimens, (b) the press-formed specimens, and (c) the annealed specimens.

Fig. 3(b) shows the resulting R-curve, representing the fracture toughness as function of the crack length. In general, all specimens exhibited a mild decrease of the G_{IC} values with increasing of the crack length. The root cause of this phenomenon is unknown. However, as the development of the R-curve is similar for all specimens, this phenomenon does not hinder sample comparison. Therefore, for each specimen, the fracture toughness was determined by calculating the average and the standard deviation of the R-curve up to a crack length value of 120 mm.

Fig. 4 summarizes the fracture toughness results and the relevant standard deviation obtained for all the specimens. It can be observed that the sample consolidated in the autoclave is characterized by an average toughness of 1.7 kJ/m^2, obtained by averaging the toughness values of the five specimens shown in Fig. 4(a). From Fig. 4(b), it is evident that the press-forming step caused an increase of the toughness to an average value of 2.2 kJ/m^2. On the other hand, the annealing step seems to have reduced the average toughness to an average value of 1.8 kJ/m^2 as shown in Fig. 4(c), which is comparable to the fracture toughness measured for the autoclave consolidated sample. These results indicate that the different thermal histories influenced the fracture toughness of titanium–PEKK interfaces. In order to get a better understanding, further analysis of PEKK degree of crystallinity and crystal morphology, along with identification of the failure mechanisms is reported in the next sections.

3.2. DSC measurements

Following DCB testing, the PEKK polymer present on the crack surfaces was analyzed by DSC. Fig. 5 shows an example of the heating and the cooling traces obtained for each sample compared to the as-received PEKK film, while Table 1 gives an overview of the results. From Fig. 5(a), it can be noticed that the as-received film exhibits a cold crystallization peak at 215 °C, whose enthalpy is close to the enthalpy of fusion. This indicates that the as-received PEKK film was characterized by a very low degree of crystallinity. The consolidation in the autoclave allowed PEKK to attain the maximum possible degree of crystallization, as no cold crystallization peak occurred before the melting peak. In contrast, the press-forming step led to a significant decrease of the degree of crystallinity, as a cold crystallization peak was observed. The annealing step caused an increase of the degree of crystallinity as the DSC trace showed a very small cold crystallization peak occurring at around 180 °C.

Overall, from Table 1, it can be observed that the three different process histories caused three different degrees of crystallinity. The autoclave consolidated sample is characterized by a highly crystallized PEKK, whereas the press-formed sample is characterized

Table 1
Overview of the DSC test results. The values represent the average and the standard deviation of three DSC specimens for each sample.

Sample	T_g (°C)	ΔH_c (J/g)	ΔH_f (J/g)	χ_c (%)	T_c (°C)
As-received	148.8 ± 0.4	25.9 ± 0.4	31.4 ± 1.3	4.2 ± 0.7	272.3 ± 1.9
Autoclave	156.0 ± 0.8	–	29.5 ± 2.2	22.3 ± 1.7	254.0 ± 2.9
Press-forming	160.1 ± 0.2	21.6 ± 0.4	27.6 ± 1.5	4.3 ± 0.7	245.5 ± 1.3
Annealing	158.8 ± 0.4	2.7 ± 1	27.0 ± 1.4	18.7 ± 1.1	245.4 ± 0.7

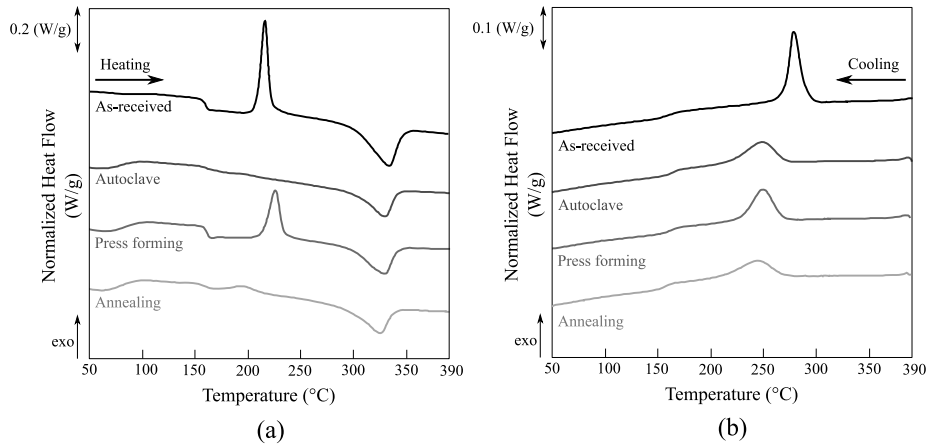

Fig. 5. Representative example of (a) the DSC heating traces and (b) the DSC cooling traces for the three samples compared to the as-received PEKK.

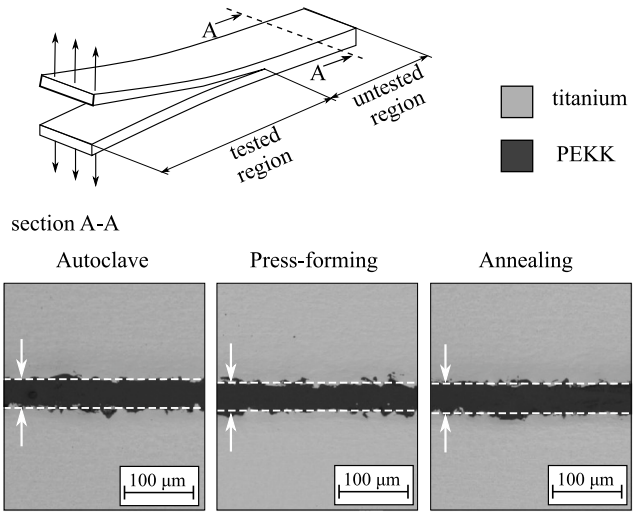

Fig. 6. Schematic illustration of the location where the cross sectional images were taken (top). Cross sectional microscopy images of an autoclaved specimen, a press-formed specimen and an annealed specimen, respectively (bottom).

by a highly amorphous PEKK. The large difference in the degree of crystallinity achieved by these two samples can be attributed to the large difference in cooling rates used. The high cooling rate used during the press-forming step, inhibited crystallization. As expected, the annealing step after press-forming promoted PEKK recrystallization, as this sample is characterized by a degree of crystallinity comparable to the value reached in the autoclave.

An additional consideration can be made by looking at T_g, ΔH_f, and crystallization temperature (T_c) during cooling. All the three samples showed an increase of T_g as well as a decrease of ΔH_f and T_c compared to the as-received PEKK. This likely indicates that PEKK was subjected to some degradation during the manufacturing process [20]. The largest drop of the crystallization temperature is observed after the first heating cycle in the autoclave, given the exposure to high temperatures for long time. Press-forming and annealing mainly caused changes in the polymer morphology without leading to a further significant degradation of the polymer.

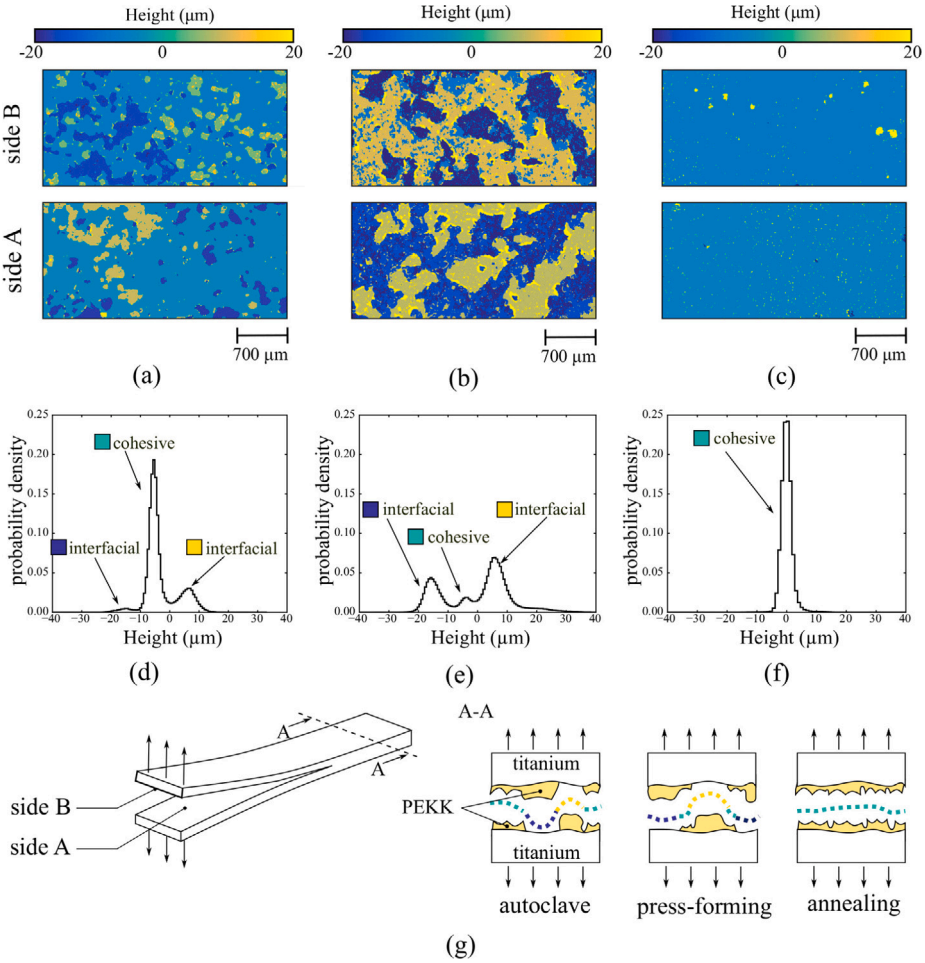

Fig. 7. (a) Height map of crack surface of an autoclave consolidated specimen, (b) height map of crack surface of a press-formed specimen, (c) height map of crack surface of an annealed specimen, (d) height distribution of crack surface of an autoclave consolidated specimen, (e) height distribution of crack surface of a press-formed specimen, (f) height distribution of crack surface of an annealed specimen, (g) schematic overview of the three different failure paths.

3.3. Cross sectional views

Cross sectional micrographs of all samples were taken at the end of the bonded region, as schematically depicted in Fig. 6. The typical cross sectional views obtained for the three types of samples are also depicted in Fig. 6. In all cases, the amount of polymer used was sufficient to fill the titanium surface irregularities, leading to a good consolidation quality, with no voids observed at the titanium–PEKK interface or within the PEKK polymer. Furthermore, all micrographs show a similar polymer thickness of about 40 µm, indicating that some polymer squeeze flow occurred during the first consolidation step in the autoclave. The additional press-forming step did not cause any further polymer squeeze flow.

3.4. Fracture surface analysis

3D optical surface microscopy was employed to identify the failure mechanisms. The analysis was carried out by scanning both sides of the fractured specimen (denoted as side A and B) at corresponding locations of the crack surface. In general, comparing side A with side B from the height maps depicted in Fig. 7, the areas having the same height are indicative of cohesive failure. Conversely, areas of opposing height, in which a peak in A approximately matches with a valley in B, indicate interfacial failure.

Fig. 7(a) shows the height map of the fracture surface of an autoclaved specimen in which both interfacial and adhesive failure can be identified. From the resulting height map in Fig. 7(d), it is evident that cohesive failure predominantly occurred. Conversely, the crack surface of a press-formed specimen is mainly characterized by interfacial failure as shown in Fig. 7(b) and (e), meaning that the crack alternately propagated at one of the two titanium–PEKK interfaces. In some limited regions, also cohesive failure is observed. In the case of the annealed sample, the crack path primarily ran through the polymer, resulting in a dominant cohesive

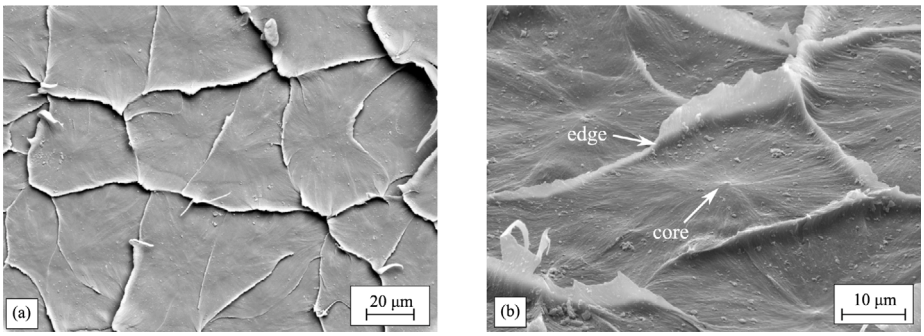

Fig. 8. (a) SEM micrograph of the fracture surface of an autoclave consolidated specimen. The micrograph was taken where cohesive failure occurred, (b) detailed image of PEKK spherulite on crack surface.

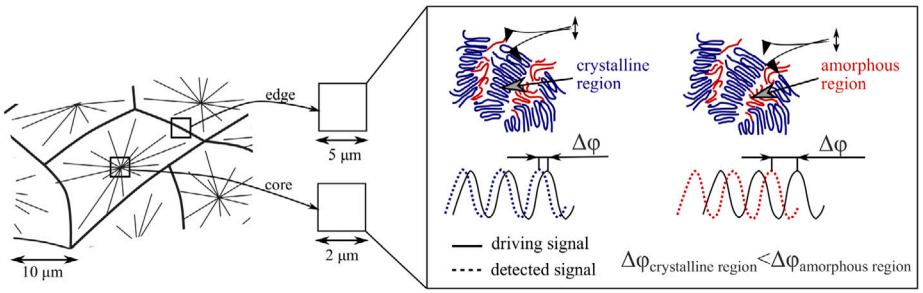

Fig. 9. Schematic representation of a spherulite with highlighted the locations where the AFM analysis was conducted.

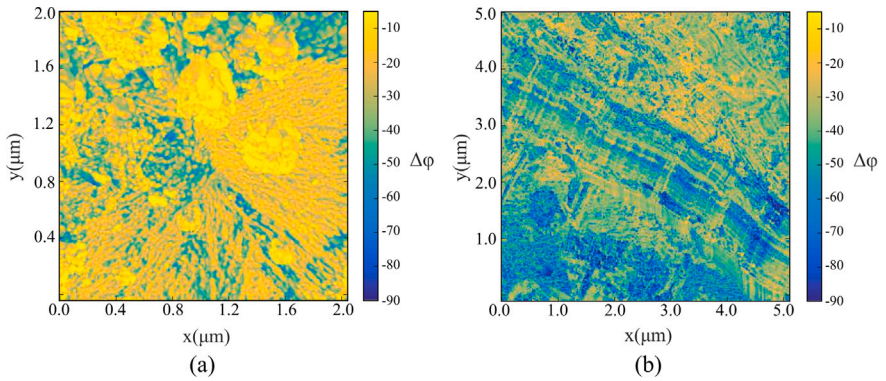

Fig. 10. AFM phase images of the fracture surface of an autoclave consolidated specimen: (a) region corresponding to the core of the spherulite (b) region corresponding to the edge of the spherulite.

failure, as depicted in Fig. 7(c) and (f). A schematic overview of the different delamination paths observed in each type of sample is summarized in Fig. 7(g).

A more in-depth analysis of the fracture surfaces was conducted using SEM and AFM. The SEM images shown in Fig. 8 provide a detailed view of the morphology of the fracture surface of a specimen consolidated in the autoclave. These micrographs show that the crack propagated through a highly crystallized PEKK, as the distinct spherulitic structure can be noticed. Fig. 8(b) shows a magnification of a PEKK spherulite, consisting of a nucleation point (core) and lamellas organized in a radial fashion. The spherulite morphology was further analyzed via AFM considering the region close to the nucleation point (core) and the spherulite boundary (edge), as schematically shown in Fig. 9.

Fig. 10(a) and (b) show the phase images obtained from the AFM analysis, depicting the phase shift ($\Delta\phi$) between driving and detected signal of the measurements carried out on the core and the edge of the spherulite, respectively.

The brighter regions (yellow) are characterized by a higher modulus and therefore, a high crystallinity content. The darker regions (blue) indicate areas characterized by a lower modulus and therefore, a low crystallinity content. The presence of the lamellas in the core of the spherulite is shown in Fig. 10(a) by the brighter regions that radially start from the center of the image. Then, each

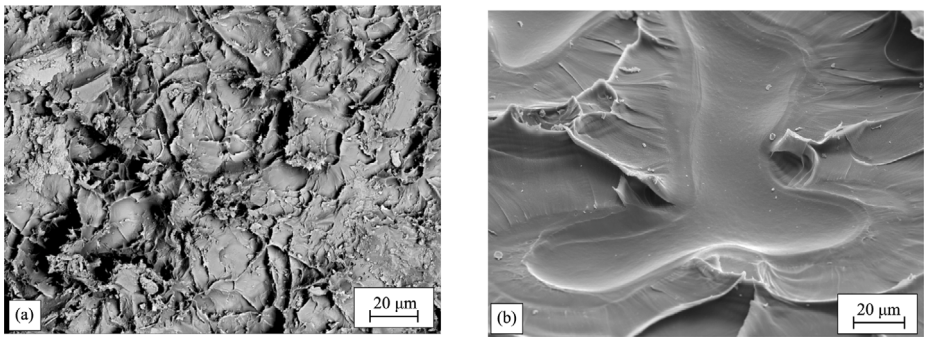

Fig. 11. SEM micrographs of the fracture surfaces of a press-formed specimen: (a) the micrograph shows the PEKK side of a region where interfacial failure occurred, (b) the micrograph shows the PEKK in the region where cohesive failure occurred.

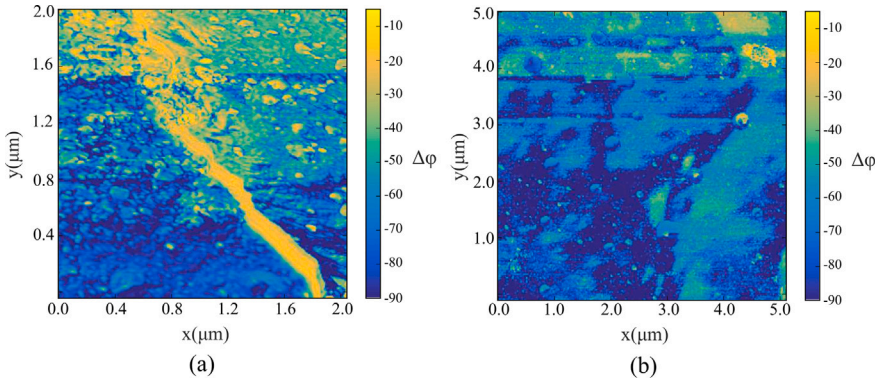

Fig. 12. AFM phase images of the fracture surfaces of a press-formed specimen: (a) region dominated by interfacial failure, (b) region dominated by cohesive failure.

lamella is alternated with amorphous polymer (interlamellar amorphous zone), which appears darker. The overall high crystallinity content of the spherulite core, resulted in regions characterized by low ductility [13]. This may explain the flat appearance of the crack surface in these regions, which suggests brittle failure.

From Fig. 10(b), it can be observed that the spherulite edge is characterized by a more amorphous polymer, as the phase image appears darker than the phase image of the spherulite core. The lower crystallinity content of the spherulite edges explains their ductile appearance, as more plastic deformation could take place.

The crack surface of a press-formed specimen was also analyzed. In the case of interfacial failure, the polymer side of the crack surface was observed, as is depicted in Fig. 11(a). The rougher appearance of the surface, compared to the autoclave consolidated specimen, suggests that more plastic deformation occurred, thereby contributing to an increase of the fracture toughness. The AFM phase imaging conducted on this area, and reported in Fig. 12(a), shows a highly amorphous polymer with some residual lamellas (brighter region in the middle), explaining the more ductile behavior compared to what was observed for the autoclave specimen.

Fig. 11(b) depicts the crack surface of the same specimen, but now for a region where cohesive failure occurred. The micrograph displays a structure similar to a pore or a void present in the polymer. The AFM analysis conducted on this region, as provided in Fig. 12(b), shows that the polymer is predominantly amorphous, with no traces of residual crystallinity detected.

The same SEM and AFM analyses were conducted on the crack surface of an annealed specimen. SEM micrographs are represented in Fig. 13, showing a similar brittle failure as observed for the autoclave consolidated specimen. As the annealing step allowed polymer recrystallization after press-forming, the crack predominantly propagated through the spherulites, characterized by a core with high crystallinity, as shown in Fig. 14(a), and more amorphous boundaries, which were plastically deformed, as shown in Fig. 14(b).

An additional analysis was conducted to characterize the PEKK crystalline morphology of the autoclave and annealed samples. For this purpose, six SEM micrographs, such as shown in Fig. 15(a) and (d), were taken at random locations from the crack surfaces of each sample. Subsequently, image thresholding and contour analysis were used to evaluate the spherulite area, as depicted in Fig. 15(b) and (e). The results are represented in terms of area-weighted distribution of the spherulites size [21], as shown Fig. 15(c) and (f). The annealed sample is characterized by a larger average spherulite size (mean diameter of 54 μm) and a wider size distribution (standard deviation of 18.7 μm) compared to the autoclaved sample (mean diameter of 42 μm and a standard deviation of 14.5 μm).

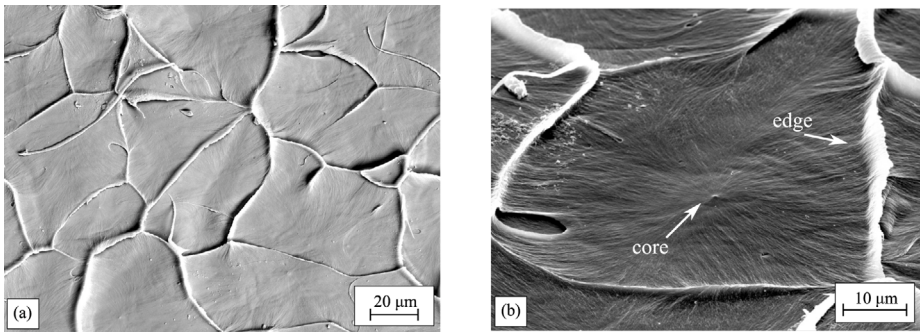

Fig. 13. (a) SEM micrograph of the fracture surface of an annealed specimen. The micrograph was taken where cohesive failure occurred, (b) detailed image of PEKK spherulite on crack surface.

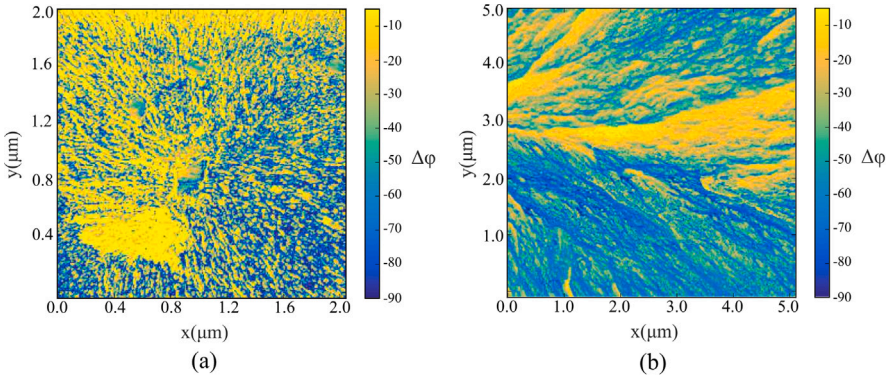

Fig. 14. AFM phase images of the fracture surface of an annealed specimen: (a) region corresponding to the core of the spherulite, (b) region corresponding to the edge of the spherulite.

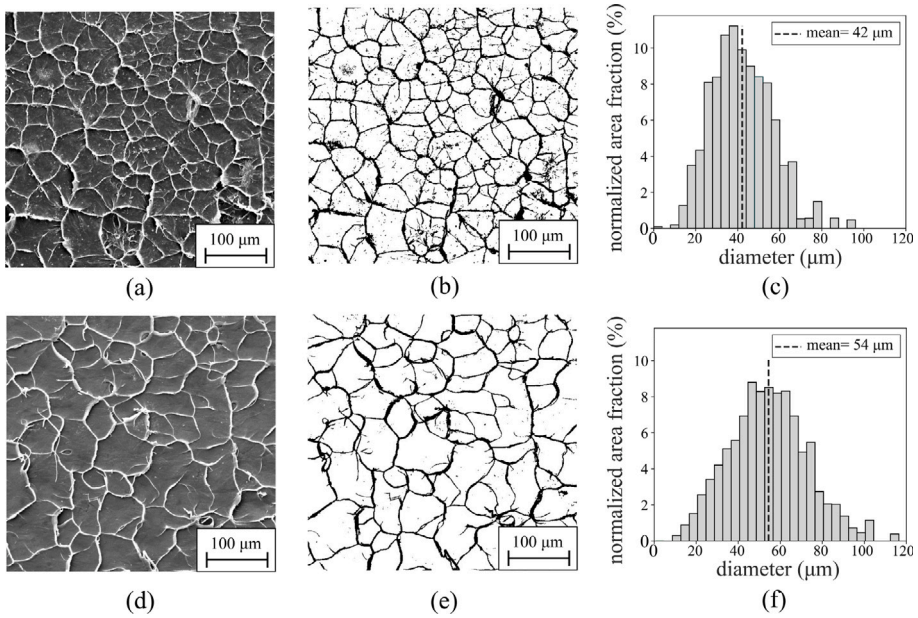

Fig. 15. (a) Example of SEM micrograph of crack surface of an autoclave consolidated specimen, (b) image thresholding of the SEM micrograph, (c) spherulite size distribution of the autoclave consolidated sample, (d) example of SEM micrograph of crack surface of an annealed specimen, (e) image thresholding of the SEM micrograph, (f) spherulite size distribution of the annealed sample.

4. Discussion

This section combines the obtained results with the purpose of gaining a better understanding of the interrelation between mechanical performance, process induced micro-scale polymer morphology, and the underlying failure mechanisms.

From the cross-sectional micrographs depicted in Fig. 6, it can be observed that all the samples are characterized by a comparable polymer thickness of about 40 μm. This result allows to rule out the influence of polymer thickness on the fracture toughness [14,22], thereby attributing the measured differences to the degree of crystallinity and polymer morphology generated by the different processes.

In general, the autoclave and annealed samples, characterized by a highly crystallized PEKK, exhibited a lower fracture toughness than the press-formed sample, which was characterized by a highly amorphous PEKK. Fracture analysis conducted with SEM and AFM showed that, in the autoclave and annealed samples, the failure path mostly propagated through the PEKK spherulites, which consisted of a highly crystallized core surrounded by an amorphous phase. The type of fracture observed suggests that the polymer crystallized from the bulk [12], meaning that homogeneous crystallization occurred. The homogeneous crystallization may also explain the relatively large size of the spherulites observed, which is a result of a low nucleation density within the polymer bulk. For this material system, the titanium surface did not seem to promote any heterogeneous crystallization at the interface. If heterogeneous crystallization had taken place, then this phenomenon would have been detected during crack surface analysis, as it leads to the formation of a lamellar crystalline polymer interphase between metal and polymer bulk. Typically, this interphase layer represents the weakest point in the polymer, hence its presence would strongly influence the fracture behavior [23]. Overall, this type of crystallization behavior influenced the type of failure mechanism that occurred, as the crack preferably propagated through the spherulite structures [24], other than the interface. Hence, the lower toughness can be mostly related to the brittle fracture caused by the spherulites, with a low contribution of the amorphous edges that caused some plastic deformation, thereby a more ductile failure.

Image thresholding shown in Fig. 15 allowed to estimate the amount of plastic deformation in terms of surface fraction taken up by the spherulite boundaries. It was found an amount of ductile failure of approximately 15% for all the SEM micrographs taken from both samples. This result may explain the comparable mechanical response of autoclaved and annealed samples, despite their difference in crystalline morphology also reported in Fig. 15. Assuming that the toughness of the crystalline and amorphous regions are independent on the processing history, the measured toughness of the samples would depend on the area fraction between crystalline and amorphous regions. Or, more concretely, on the ratio between spherulite area and spherulite edge length in these images.

The fracture analysis conducted on the press-formed sample shows a predominant interfacial failure, despite this sample exhibits a higher toughness. A first explanation for this type of mechanical response is that by quench-cooling PEKK during press-forming, the toughness of PEKK significantly increased due to the increase of the amorphous phase [25]. As a consequence, the titanium–polymer interface became the weakest link, resulting in interfacial failure. The enhanced toughness is related to the increased ability of the amorphous PEKK to plastically deform, as suggested by Fig. 11(a), where the plastic deformation of PEKK is visible on the entire inspected area. In contrast, for the autoclave and annealed samples, the plastic deformation of PEKK is a phenomenon limited to the spherulite boundaries, as shown in Figs. 8 and 13. A second explanation is that the fast cooling rate caused a decrease of the interfacial adhesion and a local bridging of PEKK during delamination. Consequently, the local bridging led to a larger toughness [26,27]. This mechanism may explain what observed in Fig. 7(b), in which the crack alternately propagated at one of the two titanium–PEKK interfaces.

The crack surface analysis conducted on the press-formed samples on the area of cohesive failure, as provided in Fig. 11(b), shows structures resembling pores or voids formed in the polymer. The cause of these pores is unclear. The first hypothesis is that the high cooling rates used during press-forming, in combination with the difference in thermal expansion between the titanium and the polymer, led to the formation of micro voids, however, the cross sectional micrographs examined did not reveal the presence of such voids. The second hypothesis is that the presence of the amorphous polymer enabled the cavitation phenomenon followed by void coalescence, which occurs in high toughness polymers when they are subjected to nearly hydrostatic tensile stress [28,29]. Under this type of load, a void is formed at the crack tip when the crack propagates in the amorphous phase of the polymer [30]. Further research is required on the manufacturing of these type of joints with high cooling rates to better understand the mechanisms leading to the enhanced toughness as well as the source of porosity.

Overall, our results confirm that the processing history has a significant influence on the polymer microstructure and therefore on the toughness of titanium–PEKK interfaces. A slow process or an annealing step generally causes a high degree of crystallinity, which results in primarily brittle failure and therefore, in a lower fracture toughness. Conversely, a fast process seems to be preferable, as the presence of an amorphous polymer at the interface is beneficial to increase the fracture toughness. However, it is also well known that a fully amorphous polymer is not recommended due to its low environmental resistance [31], which may be detrimental to the interfacial bond in presence of moisture or other substances. Ideally, it would be desirable to maintain a high degree of crystallinity, but increase the amount of plastic deformation. This can be achieved by reducing the spherulite size to maximize the amount of the spherulite edge length and hence, the amount of ductile fracture. Given that titanium does not promote polymer crystallization, nucleating agents or nanoparticles [23] may be employed to promote higher nucleation and crystallization density.

5. Conclusions

The present work investigated the interrelation between thermal history, polymer morphology, and fracture toughness of titanium–PEKK interfaces. Samples were prepared with three manufacturing technologies, namely: autoclave consolidation, press-forming and annealing. Autoclave consolidation represents slow processes, characterized by low cooling rates, whereas, press-forming represents fast processes, characterized by high cooling rates. The annealing step was carried out to allow recrystallization after fast cooling.

DSC tests showed that the slow cooling during autoclave consolidation, as well as the annealing step, caused PEKK to reach a high degree of crystallinity. Conversely, the fast cooling during press-forming led to a mainly amorphous polymer. Microscopy conducted on the fracture surfaces may indicate that the crystallization morphology was not affected by the titanium surface. The presence of large spherulites suggested that PEKK crystallized from the bulk, thereby having homogeneous crystallization.

The combination of DCB results and fracture surface analysis showed that the process-induced morphology influenced the failure mechanisms, and consequently, the fracture toughness. The autoclaved and annealed specimens predominantly showed cohesive failure. The crack propagated mostly through the PEKK spherulites, involving a combination of brittle failure (core of the spherulite) and ductile failure (spherulite boundaries). This type of failure resulted in a lower fracture toughness than the press-formed specimens. These specimens predominantly showed interfacial failure, involving extensive plastic deformation of the amorphous PEKK polymer.

CRediT authorship contribution statement

V.M. Marinosci: Writing – original draft, Methodology, Investigation, Formal analysis, Data curation, Conceptualization. **N.G.J. Helthuis:** Investigation, Methodology. **L. Chu:** Writing – review & editing, Investigation, Formal analysis. **W.J.B. Grouve:** Supervision, Writing – review & editing, Conceptualization. **M.B. de Rooij:** Conceptualization, Supervision, Writing – review & editing. **S. Wijskamp:** Writing – review & editing, Supervision, Conceptualization. **R. Akkerman:** Project administration, Writing – review & editing.

Declaration of competing interest

The authors declare that they have no known competing financial interests or personal relationships that could have appeared to influence the work reported in this paper.

Acknowledgments

This research was carried out under project number 16213 funded by the Dutch Research Council (NWO), Netherlands. The authors gratefully acknowledge the financial and technical support from the industrial and academic members of the ThermoPlastic composites Research Center (TPRC), Netherlands, as well as the support funding from the Province of Overijssel, Netherlands for improving the regional knowledge position within the Technology Base Twente initiative.

References

[1] Akbarpour S, Hallström S. Reinforcement around holes in composite materials by use of patched metal inserts. Compos Struct 2019;225:111084.
[2] Mehta K. Advanced joining and welding techniques: an overview. Adv Manufact Technol 2017;101–36.
[3] Dadej K, Bieniaś J, Surowska B. Residual fatigue life of carbon fibre aluminium laminates. Int J Fatigue 2017;100:94–104.
[4] Fink A, Kolesnikov B. Hybrid titanium composite material improving composite structure coupling. In: Spacecraft Structures, Materials and Mechanical Testing 2005, vol. 581. 2005.
[5] Reynolds N, Awang-Ngah S, Williams G, Hughes D. Direct processing of structural thermoplastic composites using rapid isothermal stamp forming. Appl Compos Mater 2020;27(1):107–15.
[6] Vincent GA, de Bruijn TA, Wijskamp S, Rasheed MIA, van Drongelen M, Akkerman R. Shredding and sieving thermoplastic composite scrap: Method development and analyses of the fibre length distributions. Composites B 2019;176:107197.
[7] Baldan A. Adhesively-bonded joints and repairs in metallic alloys, polymers and composite materials: Adhesives, adhesion theories and surface pretreatment. J Mater Sci 2004;39(1):1–49.
[8] Ji C, Wang B, Hu J, Sun Y, et al. Effect of different preparation methods on mechanical behaviors of carbon fiber-reinforced PEEK-Titanium hybrid laminates. Polym Test 2020;85:106462.
[9] Molitor P, Barron V, Young T. Surface treatment of titanium for adhesive bonding to polymer composites: a review. Int J Adhes Adhes 2001;21(2):129–36.
[10] Su Y, de Rooij M, Grouve W, Akkerman R. The effect of titanium surface treatment on the interfacial strength of titanium–Thermoplastic composite joints. Int J Adhes Adhes 2017;72:98–108.
[11] Marinosci VM, Grouve WJ, de Rooij MB, Wijskamp S, Akkerman R. Effect of grit-blasting on the fracture toughness of hybrid titanium-thermoplastic composite joints. Int J Adhes Adhes 2021;109:102893.
[12] Garcia-Leiner M, Reitman MT, El-Hibri MJ, Roeder RK. Structure-property relationships in commercial polyetheretherketone resins. Polym Eng Sci 2017;57(9):955–64.
[13] Gao S-L, Kim J-K. Cooling rate influences in carbon fibre/ PEEK composites. Part I. Crystallinity and interface adhesion. Composites A 2000;31(6):517–30.
[14] Sacchetti F, Grouve WJ, Warnet LL, Villegas IF. Effect of cooling rate on the interlaminar fracture toughness of unidirectional carbon/PPS laminates. Eng Fract Mech 2018;203:126–36.
[15] Bassett D, Olley R, Al Raheil I. On crystallization phenomena in PEEK. Polymer 1988;29(10):1745–54.
[16] Magonov S, Elings V, Whangbo M-H. Phase imaging and stiffness in tapping-mode atomic force microscopy. Surf Sci 1997;375(2–3):L385–91.

[17] Hobbs JK, Farrance OE, Kailas L. How atomic force microscopy has contributed to our understanding of polymer crystallization. Polymer 2009;50(18):4281–92.
[18] Chu L, Grouve WJ, van Drongelen M, de Vries EG, Akkerman R, de Rooij MB. Formation of flat-on lamellar crystals in absence of nanoconfinement. Adv Mater Interf 2021;8(7):2001894.
[19] Williams J. Introduction to linear elastic fracture mechanics. 2001.
[20] Pascual A, Toma M, Tsotra P, Grob MC. On the stability of PEEK for short processing cycles at high temperatures and oxygen-containing atmosphere. Polym Degrad Stab 2019;165:161–9.
[21] Lopez-Sanchez MA. GrainSizeTools: a python script for grain size analysis and paleopiezometry based on grain size. J Open Source Softw 2018;3(30):863.
[22] Fernandes RL, de Freitas ST, Budzik MK, Poulis JA, Benedictus R. From thin to extra-thick adhesive layer thicknesses: fracture of bonded joints under mode I loading conditions. Eng Fract Mech 2019;218:106607.
[23] Chu L, Grouve WJ, van Drongelen M, Guha Y, de Vries EG, Akkerman R, de Rooij MB. Influence of the polymer interphase structure on the interaction between metal and semicrystalline thermoplastics. Adv Energy Mater 2021;23(2):2000518.
[24] Li J-Z, Schultz JM, Chan C-M. The relationship between morphology and impact toughness of poly (L-lactic acid)/poly (ethylene oxide) blends. Polymer 2015;63:179–88.
[25] Gao S-L, Kim J-K. Cooling rate influences in carbon fibre PEEK composites. Part II: interlaminar fracture toughness. Composites A 2001;32(6):763–74.
[26] Tao R, Li X, Yudhanto A, Alfano M, Lubineau G. Laser-based interfacial patterning enables toughening of CFRP/epoxy joints through bridging of adhesive ligaments. Composites A 2020;139:106094.
[27] Li X, Tao R, Alfano M, Lubineau G. How variability in interfacial properties results in tougher bonded composite joints by triggering bridging. Int J Solids Struct 2020;191:87–98.
[28] Lu Y, Men Y-F. Initiation, development and stabilization of cavities during tensile deformation of semicrystalline polymers. Chinese J Polymer Sci 2018;36(10):1195–9.
[29] Greenhalgh E. Failure Analysis and Fractography of Polymer Composites. Elsevier; 2009.
[30] Mahajan DK, Singh B, Basu S. Void nucleation and disentanglement in glassy amorphous polymers. Phys Rev E 2010;82(1):011803.
[31] Negoro T, Thodsaratpreeyakul W, Takada Y, Thumsorn S, Inoya H, Hamada H. Role of crystallinity on moisture absorption and mechanical performance of recycled PET compounds. Energy Procedia 2016;89:323–7.